High Pressure Research
Vol. 32, No. 2, June 2012, 239–254

Taylor & Francis
Taylor & Francis Group

A large volume cubic press with a pressure-generating capability up to about 10 GPa

Xi Liu[a,b]*, Jinlan Chen[a,b,c], Junjie Tang[a,b], Qiang He[a,b], Sicheng Li[a,b,c], Fang Peng[d], Duanwei He[d], Lifei Zhang[a,b] and Yingwei Fei[a,b,e]

[a]*Key Laboratory of Orogenic Belts and Crustal Evolution, Ministry of Education of China, Beijing, People's Republic of China;* [b]*School of Earth and Space Sciences, Peking University, Beijing 100871, Beijing, People's Republic of China;* [c]*Henan Sifang Diamond Co., Ltd, Zhengzhou 450016, People's Republic of China;* [d]*Institute of Atomic and Molecular Physics, Sichuan University, Chengdu 610065, People's Republic of China;* [e]*Geophysical Laboratory, Carnegie Institution of Washington, 5251 Broad Branch Road, NW, Washington, DC 20015, USA*

(*Received 19 August 2011; final version received 11 January 2012*)

A massive cubic press, with a maximum load of 1400 tons on every WC anvil, has been installed at the High Pressure Laboratory of Peking University. High-*P* experiments have been conducted to examine the performance of the conventional experimental setup and some newly developed assemblies adopting the anvil-preformed gasket system. The experimental results suggest that (1) the conventional experimental setup (assembly BJC2-0) can reach pressures up to about 6 GPa with a large cell volume of 34.33 cm^3; (2) the anvil-preformed gasket system, despite decreasing the *P*-generating efficiency, extends the *P*-generating capability up to about 8 GPa at the expense of reducing the cell volume down to 8.62 cm^3 (assembly BJC2-6); (3) due to the large cell volume, it is possible to make further modifications to extend the pressure range, as readily demonstrated, to about 10 GPa (assembly BJC5-7); (4) the effect of high temperature on the pressure generation of the press is not significant. It follows that this cubic press can be very useful in synthesizing materials of large volume at high pressures and to the studies such as high-*P* phase equilibrium, trace element partitioning and isotope fractionation in the research fields of Earth and planetary sciences.

Keywords: cubic press; large volume; *P*-generating capability; *P*-generating efficiency

1. Introduction

Simulating the high-*P* and high-*T* conditions of the deep interiors of the Earth and other planetary bodies is crucial for the studies of Earth and planetary sciences, which has been a constant driving force in developing new high-*P* experimental techniques. Nowadays the routinely used high-*P* equipments include cold-seal pressure vessel [1,2], internally heated gas vessel [3,4], piston–cylinder apparatus [5–7], multi-anvil press [8–10] and diamond-anvil cell [11–13]. The application of the cold-seal pressure vessel and internally heated gas vessel is usually limited to low pressures ($\leq$1 GPa). The piston–cylinder apparatus has a similar problem, a low *P*-generating

*Corresponding author. Email: xi.liu@pku.edu.cn

ISSN 0895-7959 print/ISSN 1477-2299 online

http://dx.doi.org/10.1080/08957959.2012.657634
http://www.tandfonline.com

capability, which is often less than 3 GPa [6,14], and only occasionally up to 5 GPa [7]. Taking into account the vast pressure ranges encountered in the interiors of the Earth and other planetary bodies (*e.g.* about 23 GPa at the upper mantle–lower mantle boundary of the Earth), other high-*P* experimental techniques are apparently needed. No doubt that the diamond-anvil cell can generate extremely high pressures (∼550 GPa [15]) and has been widely used in the investigations of phase transition [16], equation of state [13], electrical impedance [17], etc. Its extremely small sample size, however, limits its application in the Earth and planetary sciences, so that studies in the research fields such as phase equilibrium and element partitioning have been rarely carried out with the diamond-anvil cell [18,19].

The multi-anvil press is well known as the high-*P* equipment which can maintain a reasonably large sample size and achieve relatively high pressures at the same time. The generation of high pressure in the multi-anvil press is very complicated and largely dependent on the factors such as the material of the second-stage anvils (WC or sintered diamond), the truncation edge length of the second-stage anvils, the size of the octahedral pressure medium, and the dimensional specifics of the pyrophyllite gaskets. With WC as its second-stage anvils, the maximum achievable pressure by the multi-anvil press is about 30 GPa [20,21]; with sintered diamond as the second-stage anvils, much higher pressure can be obtained, and the present record is about 100 GPa [22]. The volume of the sample from the multi-anvil press is primarily decided by the truncation edge length and the octahedral pressure medium, which are unfavourably inversely correlated to pressure. If we use WC cubes as the second-stage anvils of a normally sized multi-anvil press (1000–2000 ton; metric tons are used in this investigation), the volume of the sample is typically in the ranges of 12 mm^3 at 4–10 GPa, 5–8 mm^3 at 11–16 GPa, 3 mm^3 at 17–21 GPa, and 1 mm^3 at 22–26 GPa [23]. Compared to the size of the samples from the cold-seal pressure vessel, internally heated gas vessel and piston–cylinder apparatus, the size of the sample from the multi-anvil press is very small, so that some experimental techniques such as the standard oxygen fugacity-buffering technique with double capsules is not applicable to most multi-anvil presses. Also a large sample size can help to reduce the thermal gradient which might be vital to some research fields such

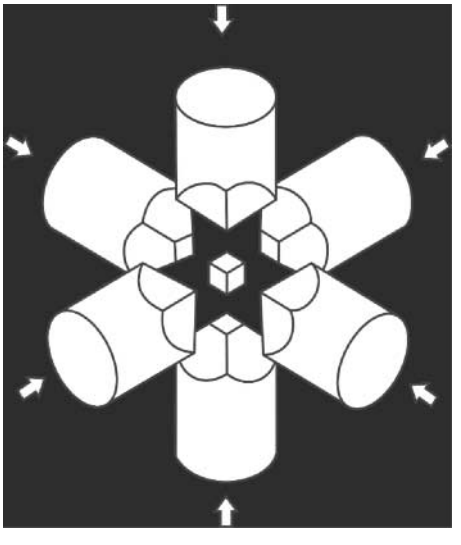

Figure 1. Sketch of the pressurizing system of the CS-IV 6 × 14 MN cubic press. To generate high pressure, six WC anvils driven by a computer-controlled hydraulic system press the central cube from three dimensions. The maximum load on every WC anvil is approximately 1400 tons (the maximum oil pressure is 100 MPa while the diameter of the individual ram is 0.42 m), which equals to a load of 4200 tons in the uniaxial press system commonly adopted by the multi-anvil press. The six rams, supporting the WC anvils, can either be operated simultaneously or individually.

as isotope fractionation [24]. In addition, many modern analysis techniques such as neutron diffraction, calorimetry measurement and nuclear magnetic resonance require large sample size, which can only be produced by duplicated experiments with the normally sized multi-anvil press or by experimenting with the overwhelming USSA-5000 press at the Institute for Study of the Earth's Interior (Okayama University, Japan) and the 5000t hydraulic press at the Bayerisches Geoinstitut, Germany [25].

Another less well-known high-*P* equipment is the cubic press, which is usually used to synthesize materials of large volume at pressures up to about 10 GPa [26–29]. Compared to the multi-anvil press, the cubic press has some advantages: the fast rate of increasing and decreasing pressure [30], the relatively simple experimental assembly arrangement, and the relatively large sample volume [31]. In contrast to its rarity in other countries, the cubic press is very popular in China and is actually the main working horse of the synthetic diamond industry which presently produces synthetic diamonds of about 1000 tons annually [30].

In 2010, the High Pressure Laboratory of Peking University installed a massive cubic press with a maximum load of about 1400 tons on every WC anvil (CS-IV 6 × 14 MN; Figure 1), which equals to a press load of 4200 tons in the common uniaxial press system adopted by most multi-anvil presses. Here, we report our progress in the new cell design, pressure calibration, and *P*-generating efficiency investigation.

2. Experiments

In the original design of the CS-IV 6 × 14 MN cubic press, the square-shaped tip of the WC anvil is of 23.5 × 23.5 mm^2, the maximum oil pressure is 100 MPa and the central pyrophyllite block is of 32.5 × 32.5 × 32.5 mm^3. The pyrophyllite block serves as both pressure medium and gasket material. According to the practice in [31], this conventional experimental setup can successfully generate a cell pressure of 5.5 GPa at a press load of about 5.5 MN (*i.e.* 560 tons), but cannot go to much higher pressure since the correlation curve of cell pressure and press load quickly levels off thereafter. On the other hand, a finite element calculation [32] suggested that the von Mises stress along the bevel of the anvil reaches about 11 GPa when the cell pressure is 5.6 GPa, indicating that most loading force is actually consumed by the pyrophyllite gasket. If higher cell pressure is the target, then much higher press load is necessary, which unfortunately increases the potentiality in breaking the whole WC anvils and subsequently increases the experimental cost.

To increase the *P*-generating capability of the cubic press and decrease the experimental cost at the same time, an anvil-preformed gasket system has been developed [31]. The strategy in the anvil-preformed gasket system is that we add six WC pressure-enhancing blocks (WC-PEBs; Figure 2(a) and (b)) to the pyrophyllite block, as shown in Figure 2(c). As the WC-PEBs are getting thicker, their square-shaped tips are getting smaller (from 5.52 to 3.57, 2.04 and 0.94 cm^2), so that much lower press load is needed for generating similar cell pressures, or similar press loads can generate much higher cell pressure. Since the six WC main anvils do not bear any extreme pressure, they are generally risk-free, leading to a low experimental cost. During an experiment at very high pressures, the WC-PEBs might break; since they are very small in volume and low in cost, this is unimportant. One apparent disadvantage with the anvil-preformed gasket system is the sacrifice of some cell volume, now occupied by the WC-PEBs, which is not critical, thanks to the massive size of our cubic press. In addition, the anvil-preformed gasket system introduces some extra pyrophyllite gasket material (Figure 2(c)), which helps us to align the WC-PEBs but certainly consumes some press load. As the thickness of WC-PEBs increases from 0 to 2, 4 and 6 mm, the volume of the extra pyrophyllite gasket material increases from 0 to 6.00, 11.11 and 15.45 cm^3. Correspondingly, the volume of the conventional pyrophyllite cube (cell volume)

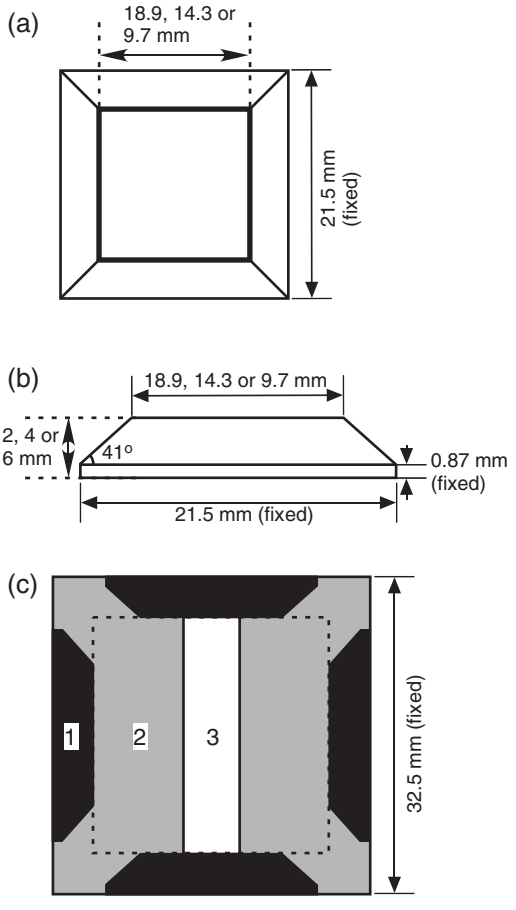

Figure 2. Drawings of the WC-PEB ((a) view from the top; (b) side view) and the central composite cube mainly consisting of six WC-PEBs and one pre-formed pyrophyllite block which serves as pressure medium and gasket (c). Numbers in (a) and (b) are the sizes of three kinds of WC-PEBs with their thickness as 2, 4 and 6 mm, respectively. In (c), part 1 is the WC-PEBs, part 2 the pyrophyllite block, and part 3 the inner cylindrical experimental unit which is enlarged and detailed in Figure 3. The pyrophyllite block consists of two components as divided by the broken square, with the inner component as the conventional pyrophyllite cube used in the original design of the cubic press and the outer component as an extra gasket material which hosts and aligns the WC-PEBs.

decreases from 34.33 to 23.15, 14.71 and 8.62 cm^3, which is still very large, compared to the octahedral pressure cell used in the multi-anvil press.

The inner cylindrical experimental unit of the assembly (part 3 in Figure 2(c)) is detailed in Figure 3. Factors here which may significantly affect the *P*-generating capability are related to the pressure-enhancing plugs (PEPs): their presence or not, their material properties and their size.

Four sets of assemblies have been developed and experimentally examined at ambient temperature to investigate the factors which potentially affect the *P*-generating efficiency of the cubic press (Table 1). The first set of assemblies is used to illustrate the effect of the different sizes of the WC-PEBs without using PEPs of any kind; these assemblies are termed as BJC2-0, BJC2-2, BJC2-4 and BJC2-6, with the second digit indicating the thickness of the WC-PEBs. The second set of assemblies is used to demonstrate the effect of the different sizes of the WC-PEBs with the presence of a 5 mm thick steel PEPs; these assemblies are termed as BJC3-0, BJC3-2, BJC3-4

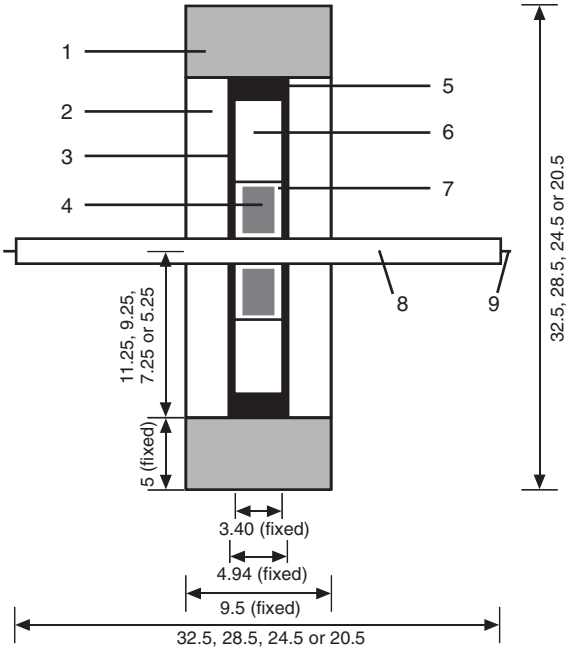

Figure 3. Schematic illustration of the inner cylindrical experimental unit. Its small components are 1, PEPs made of either steel 55 or WC (grade K30-08); 2, MgO sleeve; 3, graphite heater; 4, noble capsule with experimental charge; 5, disc of graphite or zirconia; 6, MgO spacer; 7, MgO or *h*BN cup; 8, MgO or Al_2O_3 tubing; 9, T/C wires. The shown sizes of the components are for the second set of assemblies and third set of assemblies only. For the first set of assemblies without the PEPs, the length of the MgO sleeve, graphite heater and MgO spacer is correspondingly adjusted (Table 1). For the fourth set of assemblies with the WC-PEPs of various sizes, modification is also required.

Table 1. Assemblies examined in this investigation.

	PEPs[a]		Size of WC-PEBs[b] (mm)			
Assembly set	Type	Size (mm)	0	2	4	6
First set	–	–	BJC2-0	BJC2-2	BJC2-4	BJC2-6[c]
Second set	Steel[d]	5	BJC3-0	BJC3-2	BJC3-4	BJC3-6
Third set	WC[e]	5	BJC4-0	BJC4-2	BJC4-4	BJC4-6[f]
Fourth set	–	–	–	–	–	BJC5-0[c]
	WC	3	–	–	–	BJC5-3
	WC	5	–	–	–	BJC5-5[f]
	WC	7	–	–	–	BJC5-7

[a]Pressure-enhancing plugs with size characterized by their thickness.
[b]Pressure-enhancing blocks with size characterized by their thickness.
[c]Assemblies BJC2-6 and BJC5-0 are identical.
[d]Steel 55.
[e]WC K30-08.
[f]Assemblies BJC4-6 and BJC5-5 are identical.

and BJC3-6, with the second digit similarly indicating the thickness of the WC-PEBs. The third set of assemblies is used to explore the effect of the different sizes of the WC-PEBs with the presence of a 5 mm thick WC-PEPs; these assemblies are termed as BJC4-0, BJC4-2, BJC4-4 and BJC4-6, with the second digit again indicating the thickness of the WC-PEBs. Putting these three sets of assemblies together, we can tell whether the PEPs affect the cell pressure or not, and how their material properties function. The fourth set of assemblies is used to clarify the effect of

the size of the WC-PEPs with the presence of a 6 mm thick WC-PEBs; the assemblies are termed as BJC5-0, BJC5-3, BJC5-5 and BJC5-7, with the second digit indicating the thickness of the WC-PEPs, instead of the thickness of the WC-PEBs.

In the experiments mentioned above, the cell pressures were determined by using the phase transitions of Bi (I–II transition at 2.55 GPa, II and III transition at 2.69 GPa and III–V transition at 7.7 GPa), Ba (I–II transition at 5.5 GPa) and ZnTe (band gap change at 6.6 GPa and I–II transition at 8.9 GPa) [33–36]. The phase transitions were detected using the resistance measurement method described in [37].

Additionally, the assembly BJC2-0 was used to assess the effect of temperature on its pressure generation. We conducted extensive high-P and high-T experiments about the phase boundary between quartz (Qtz) and coesite (Coe). In every experiment, two samples, with the starting material of one sample being quartz and that of the other being coesite previously synthesized at 4 GPa and 1000°C using the assembly BJC-1 [38], were run simultaneously, so that the phase boundary was reversed. Arc-welded Pt capsules, approximately 2 mm long, were used to host the experimental charges. The traditional quenching method was adopted here, with press load increased first, temperature then increased to a target value with the control of a type B thermocouple and experiment finally quenched quickly by turning off the electric power supply and then decompressed to ambient temperature. After the experimentation, the Pt capsules were manually opened, and the experimental charges were analysed by using a micro-Raman system (Renishaw system RM-1000 [39]).

3. Results

The experimental details are summarized in Tables 2–6, and the results are graphically shown in Figures 4–8. The ideal cell pressure (P_i) shown in the tables was calculated by assuming no loading force consumed by the pyrophyllite block and by assuming the WC-PEBs and WC anvils

Table 2. Efficiency of pressure generation of the first set of assemblies (BJC2-0, -2, -4 and -6).

Oil P (MPa)	Load (ton)[a]	PEB[b] (mm)	P_m (GPa)	P_i (GPa)	Efficiency (%)
Assembly BJC2-0					
16.66	236	23.5	2.55	4.18	61.0
18.31	259	23.5	2.69	4.59	58.6
58.71	830	23.5	5.5	14.73	37.3
Assembly BJC2-2					
12.55	177	18.9	2.55	4.87	52.4
14.26	202	18.9	2.69	5.53	48.6
40.61	574	18.9	5.5	15.75	34.9
Assembly BJC2-4					
9.94	141	14.3	2.55	6.73	37.9
10.96	155	14.3	2.69	7.43	36.2
36.84	521	14.3	5.5	24.96	22.0
Assembly BJC2-6					
9.32	132	9.7	2.55	13.72	18.6
10.64	150	9.7	2.69	15.67	17.2
33.92	480	9.7	5.5	49.95	11.0
57.95	819	9.7	7.7	85.33	9.0

Note: PEB, pressure-enhancing block.
[a]Press load on every WC anvil with the orthogonal pressing geometry. To transfer to the press load with the uniaxial pressing geometry adopted by the multi-anvil press, it should be multiplied by a factor of 3.
[b]PEBs characterized by the edge length of the square-shaped top face.

Table 3. Efficiency of pressure generation of the second set of assemblies (BJC3-0, -2, -4 and -6).

Oil P (MPa)	Load[a] (ton)	PEB[b] (mm)	P_m (GPa)	P_i (GPa)	Efficiency (%)
Assembly BJC3-0					
16.18	229	23.5	2.55	4.06	62.8
18.89	267	23.5	2.69	4.74	56.8
50.47	714	23.5	5.5	12.55	43.4
Assembly BJC3-2					
13.06	185	18.9	2.55	5.07	50.3
15.22	215	18.9	2.69	5.90	45.6
44.45	628	18.9	5.5	17.24	31.9
Assembly BJC3-4					
10.66	151	14.3	2.55	7.22	35.3
12.37	175	14.3	2.69	8.38	32.1
40.78	577	14.3	5.5	27.63	19.9
Assembly BJC3-6					
9.14	129	9.7	2.55	13.46	19.0
10.46	148	9.7	2.69	15.40	17.5
30.6	433	9.7	5.5	45.06	12.2
59.16	836	9.7	7.7	87.11	8.80

[a]Press load on every WC anvil with the orthogonal pressing geometry. To transfer to the press load with the uniaxial pressing geometry adopted by the multi-anvil press, it should be multiplied by a factor of 3.
[b]PEBs characterized by the edge length of the square-shaped top face.

Table 4. Efficiency of pressure generation of the third set of assemblies (BJC4-0, -2, -4 and -6).

Oil P (MPa)	Load[a] (ton)	PEB[b] (mm)	P_m (GPa)	P_i (GPa)	Efficiency (%)
Assembly BJC4-0					
12.84	182	23.5	2.55	3.22	79.2
14.18	200	23.5	2.69	3.56	75.6
44.47	629	23.5	5.5	11.16	49.3
Assembly BJC4-2					
11.26	159	18.9	2.55	4.37	58.4
13.2	187	18.9	2.69	5.12	52.5
40.12	567	18.9	5.5	15.56	35.4
Assembly BJC4-4					
8.85	125	14.3	2.55	6.00	42.5
10.09	143	14.3	2.69	6.84	39.4
31.4	444	14.3	5.5	21.27	25.9
Assembly BJC4-6					
5.35	76	9.7	2.55	7.88	32.4
6.01	85	9.7	2.69	8.85	30.4
18.58	263	9.7	5.5	27.36	20.1
37.5	530	9.7	7.7	55.22	13.9

[a]Press load on every WC anvil with the orthogonal pressing geometry. To transfer to the press load with the uniaxial pressing geometry adopted by the multi-anvil press, it should be multiplied by a factor of 3.
[b]PEBs characterized by the edge length of the square-shaped top face.

behaving mechanically ideally. Subsequently, the P-generating efficiency was derived from the experimentally measured pressure (P_m) and the calculated ideal pressure.

3.1. *First set of assemblies: BJC2-0, BJC2-2, BJC2-4 and BJC2-6*

For every assembly, as the oil pressure increases, the cell load increases (Table 2), the measured pressure increases (Figure 4(a)), but the P-generating efficiency decreases (Figure 4(b)). The decreasing P-generating efficiency may partially reflect the increasing non-ideal mechanical

Table 5. Efficiency of pressure generation of the 4th set of assemblies (BJC5-0, -3, -5 and -7).

Oil P (MPa)	Load[a] (ton)	PEB[b] (mm)	P_m (GPa)	P_i (GPa)	Efficiency (%)
Assembly BJC5-0					
9.32	132	9.7	2.55	13.72	18.6
10.64	150	9.7	2.69	15.67	17.2
33.92	480	9.7	5.5	49.95	11.0
57.95	819	9.7	7.7	85.33	9.0
Assembly BJC5-3					
8.5	120	9.7	2.55	12.52	20.4
9.42	133	9.7	2.69	13.87	19.4
26.56	375	9.7	5.5	39.11	14.1
50.28	711	9.7	7.7	74.04	10.4
Assembly BJC5-5					
5.35	76	9.7	2.55	7.88	32.4
6.01	85	9.7	2.69	8.85	30.4
18.58	263	9.7	5.5	27.36	20.1
37.5	530	9.7	7.7	55.22	13.9
Assembly BJC5-7					
4.21	60	9.7	2.55	6.20	41.1
13.76	195	9.7	5.5	20.26	27.2
19.18	271	9.7	6.6	28.24	23.4
23.87	337	9.7	7.7	35.15	21.9
33.8	478	9.7	8.9	49.77	17.9

[a]Press load on every WC anvil with the orthogonal pressing geometry. To transfer to the press load with the uniaxial pressing geometry adopted by the multi-anvil press, it should be multiplied by a factor of 3.
[b]PEBs characterized by the edge length of the square-shaped top face.

Table 6. Phase transition between quartz (Qtz) and coesite (Coe) determined by using the assembly BJC2-0.

					Phase identified by Raman spectroscopy[a]	
Run #	Oil P (MPa)	Load (ton)	T (°C)	t (h)	Sample 1[b]	Sample 2[c]
LMD027	15	212	800	5	Qtz	Qtz
LMD033	20	283	700	10	Qtz, Coe (minor)	Coe
LMD025	20	283	800	5	Qtz	Coe, Qtz (minor)
LMD029	20	283	900[d]	5	Qtz	Qtz, Coe (minor)
LMD023	20	283	1000	5	Qtz	Qtz
LMD022	25	353	1000	5	Coe	Coe
LMD024	25	353	1100	5	Coe	Coe
LMD028	25	353	1200[d]	4	Coe	Coe
LMD035	25	353	1400	5	Coe	Coe
LMD034	25	353	1500	5	Qtz	Coe, Qtz (minor)
LMD039	25	353	1600	2.5	Qtz	Qtz, Coe (minor)

[a]Typically 15 analyses were performed on every sample.
[b]The starting material was quartz.
[c]The starting material was coesite.
[d]Temperature was estimated using electrical power due to thermocouple failure.

behaviour of the WC material under higher pressure and partially reflect the increasing amount of gasket material extruded out from the pressure medium. As a consequence of the decreasing P-generating efficiency, the correlation curve between the press load and the cell pressure gradually levels off (Figure 4(a)) in good agreement with Wang et al. [31].

As the WC-PEBs increase their thickness, the size of their square-shaped tips shrinks from 5.52 to 3.57, 2.04 and 0.94 cm^2 (*c*. 5.9:3.8:2.2:1), which results in higher cell pressure (Figure 4(a)); for example, at the press load of about 825 tons, the cell pressure of the BJC2-0 assembly is just about 5.5 GPa, whereas that of the BJC2-6 assembly is about 7.7 GPa. The increasing rate of the

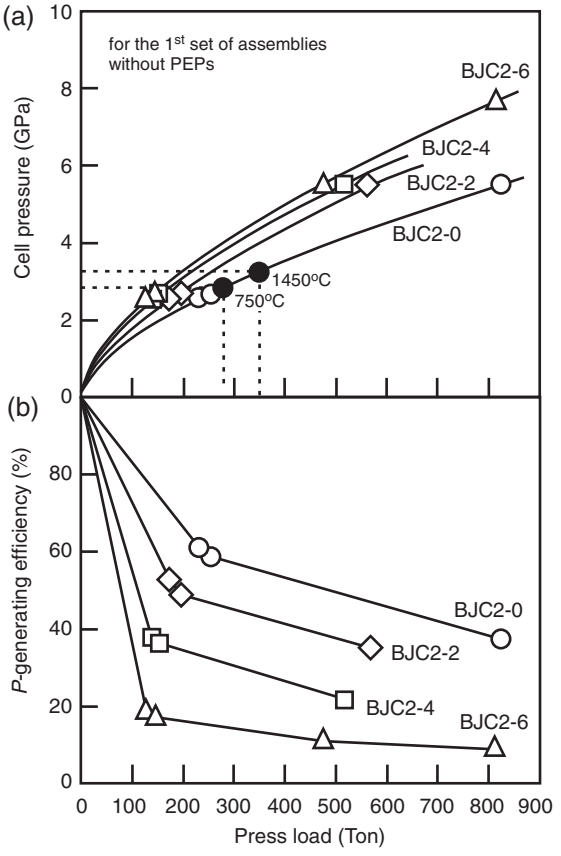

Figure 4. Cell pressure–press load relation (a) and *P*-generating efficiency (b) of the first set of assemblies (BJC2-0, BJC2-2, BJC2-4 and BJC2-6). As the WC-PEBs increase their thickness from 0 to 2, 4 and 6 mm, higher cell pressure is generated whereas the *P*-generating efficiency is decreased. The empty symbols are for the experiments at ambient temperatures, whereas those filled symbols are for the results obtained from the phase transition study between quartz and coesite at high temperatures (more discussion later). Curves are fitted by eye.

cell pressure, however, apparently does not match the decreasing rate of the area of the square-shaped tips of the WC-PEBs, suggesting increasing amount of loading force is consumed by the pyrophyllite gasket. This phenomenon is well understood by the increasing volume of the extra pyrophyllite gasket which accommodates and aligns the WC-PEBs (from 0 to 6.00, 11.11 and 15.45 cm^3). In order to increase the *P*-generating efficiency, therefore, the size of the pyrophyllite block must be reduced (more discussion later).

3.2. *Second set of assemblies: BJC3-0, BJC3-2, BJC3-4 and BJC3-6*

Very similar results of cell pressure and *P*-generating efficiency to those for the first set of assemblies have been observed for the second set of assemblies, suggesting that the 5 mm thick steel PEPs are not very useful (Figure 5).

3.3. *Third set of assemblies: BJC4-0, BJC4-2, BJC4-4 and BJC4-6*

With the 5 mm think WC PEPs, the *P*-generating capability of the third set of assemblies is substantially enhanced: for example, reaching a cell pressure of 7.7 GPa in the BJC4-6 assembly

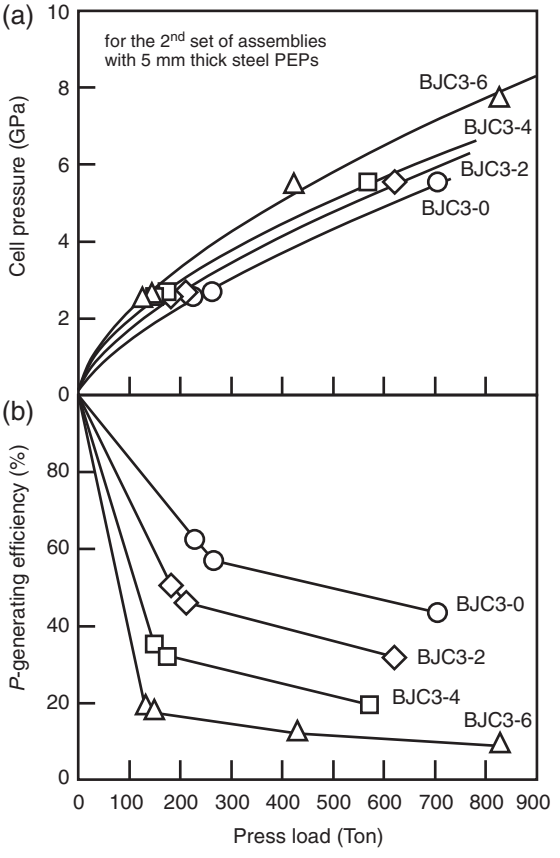

Figure 5. Cell pressure–press load relation (a) and *P*-generating efficiency (b) of the second set of assemblies (BJC3-0, BJC3-2, BJC3-4 and BJC3-6). As the WC-PEBs increase their thickness from 0 to 2, 4 and 6 mm, higher cell pressure is generated, whereas the *P*-generating efficiency is decreased. Curves are fitted by eye.

only requires a press load of about 530 tons compared to the press load of about 828 tons in both the BJC2-6 assembly and the BJC3-6 assembly (Figures 4–6). The *P*-generating efficiency is also increased significantly (*c*. 10%; compared the data in Table 4 to those in Table 3). The reason is that WC is much harder than steel.

3.4. *Fourth set of assemblies: BJC5-0, BJC5-3, BJC5-5 and BJC5-7*

Since the experiments with the third set of assemblies suggested that the WC-PEPs are able to enhance the *P*-generating capability and increase the *P*-generating efficiency, it is desirable to see how their sizes play their role.

Figure 7(a) shows that the press loads for generating similar cell pressures are significantly reduced as the thickness of the WC-PEPs increases from 0 to 3, 5, and 7 mm. Taking the cell pressure of 5.5 GPa as an example, the press load decreases from about 480 tons with the 0 mm thick WC-PEPs to 375 tons with the 3 mm thick WC-PEPs, 263 tons with the 5 mm thick WC-PEPs and 195 tons with 7 mm thick WC-PEPs. Correspondingly, the *P*-generating efficiency increases from 11.0% to 14.1%, 20.1% and 27.2% (Table 5). The phenomenon is well explained by the increasing composite bulk modulus of the assembly as the thickness of the WC-PEPs increases [31].

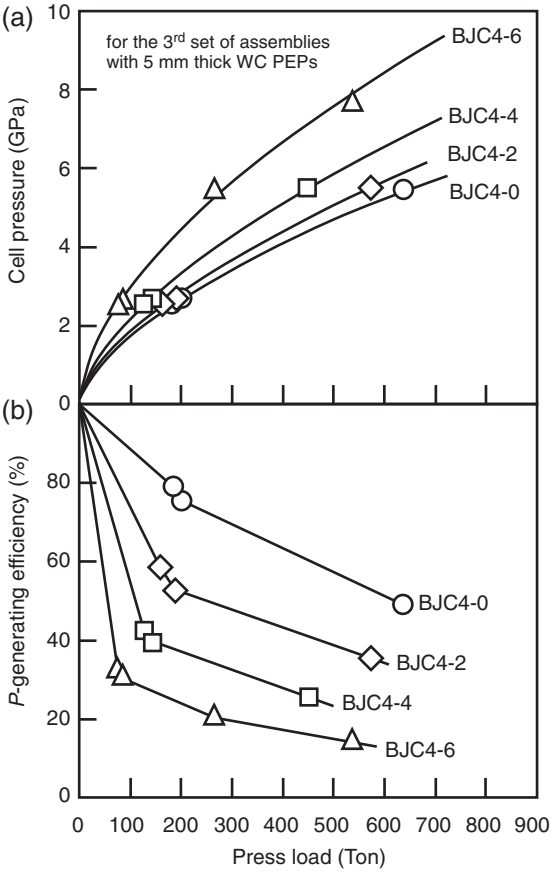

Figure 6. Cell pressure–press load relation (a) and *P*-generating efficiency (b) of the third set of assemblies (BJC4-0, BJC4-2, BJC4-4 and BJC4-6). As the WC-PEBs increase their thickness from 0 to 2, 4 and 6 mm, higher cell pressure is generated, whereas the *P*-generating efficiency is decreased. Curves are fitted by eye.

The highest cell pressure, 8.9 GPa (the transition pressure between ZnTe-I and ZnTe-II), was obtained with the assembly BJC5-7 at the press load of 478 tons, which is approximately one-third the maximum press load of our cubic press. It should be noted that this phase transition pressure has not been well established and ranges from 8.9 to 9.6 GPa [34–36]. Since Figure 7(a) shows that the correlation curve of the cell pressure and press load in the press load range of 0–478 tons is still generally linear, reaching with this assembly a cell pressure such as 10 GPa or even higher appears possible.

3.5. *Effect of high temperature on pressure generation (assembly BJC2-0)*

The experimental conditions and results about the phase transition between Qtz and Coe have been summarized in Table 6 and shown in Figure 8. The bracketed transition temperatures at the press loads of 283 and 353 tons are approximately 750°C and 1450°C, respectively. According to the latest experimental result about the phase transition between Qtz and Coe [40], these temperatures lead to the transition pressures (or cell pressure) of 2.9 and 3.4 GPa, respectively. When plotted in Figure 4, these press load–cell pressure data determined at high temperatures fall closely to the correlation curve between press load and cell pressure established at room temperature, suggesting

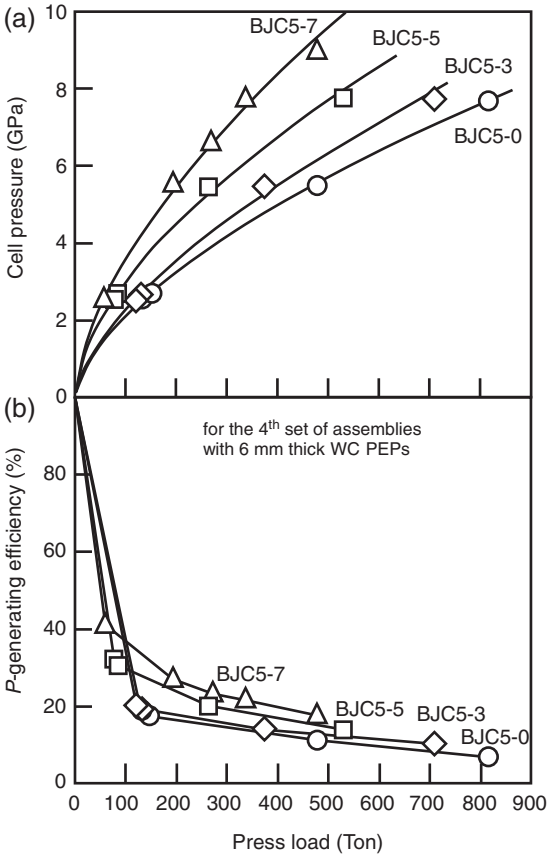

Figure 7. Cell pressure–press load relation (a) and *P*-generating efficiency (b) of the fourth set of assemblies (BJC5-0, BJC5-3, BJC5-5 and BJC5-7). In this set of assemblies, the thickness of the WC-PEBs is fixed as 6 mm, whereas the thickness of the WC-PEPs is 0, 3, 5, or 7 mm. Apparently, the WC-PEPs with increasing sizes can generate higher cell pressure and enhance the *P*-generating efficiency at the same time. Curves are fitted by eye.

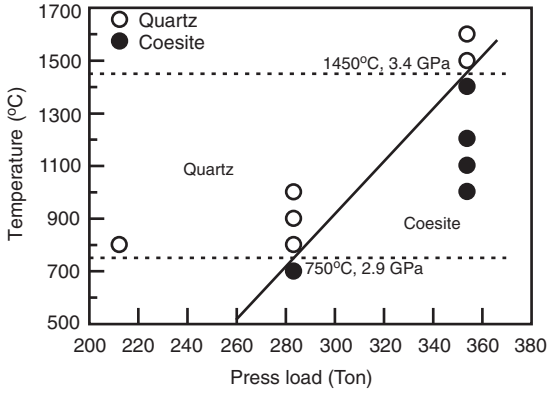

Figure 8. Reversed phase boundary between Qtz and Coe (assembly BJC2-0). Curves are fitted by eye.

that the effect of high temperature on the pressure generation of the assembly BJC2-0 is by no means significant.

4. Discussion

It is well known that generating high pressures with the equipments using solid pressure medium, such as the cubic press and multi-anvil press, is a very complicated process. For the conventional anvil-gasket system used in the cubic press [31], the size and mechanical properties of the WC anvils, and pyrophyllite pressure medium, and gasket all play roles, which leads to the levelling-off of the correlation curve of the cell pressure and press load at high pressures. In order to generate higher pressures, the most straightforward movement is to use either smaller WC anvils or larger press load, which, however, results in unbearable pressure on the WC anvils and causes a high breakage rate to them and then leads to high experimental cost [31]. With the adoption of the anvil-preformed gasket system, the damage at very high-*P* conditions is mostly done to the WC-PEBs of small volume, so that the experimental cost is substantially lowered. It is on this ground that the anvil-preformed gasket system is very successful.

However, there are disadvantages with the anvil-preformed gasket system. The adoption of the anvil-preformed gasket system obviously shrinks the volume of the conventional pyrophyllite cube; in other words, it reduces the cell volume while it increases the cell pressure. Due to the overwhelming size of our cubic press, high pressures up to about 8 GPa are readily achieved at the cell volume at least as large as 8.62 cm^3 though (the assemblage BJC2-6; Figure 4(a)). In addition, the adoption of the anvil-preformed gasket system introduces some extra pyrophyllite gasket material to the cell, which certainly consumes some press load and decreases the *P*-generating efficiency, as illustrated in Figure 9 (the first set of assemblies). If possible, therefore, the extra pyrophyllite gasket material should be reduced or even removed, as demonstrated by recent high-*P* experiments [41,42].

One potential factor which can substantially improve the *P*-generating capability and *P*-generating efficiency of the tested assemblies is to replace the WC-PEBs with the sintered diamond pressure-enhancing blocks (SD-PEBs). The Knoop hardness of the sintered diamond is about twice of that of WC [43], so that the SD-PEBs should behave more ideally than the WC-PEBs. In recent

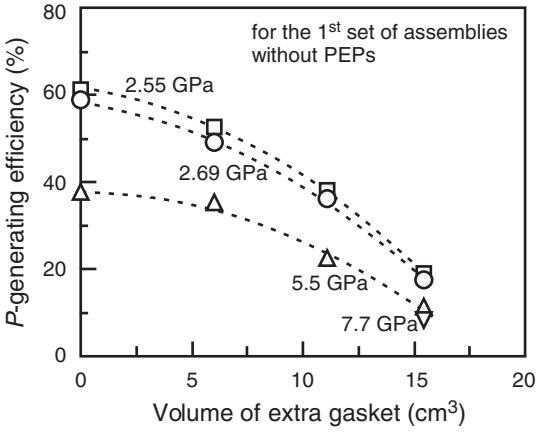

Figure 9. Effect of extra pyrophyllite gasket and pressure on *P*-generating efficiency. At low cell pressure, the influence of the extra pyrophyllite gasket on the *P*-generating efficiency is very large, but it decreases as the cell pressure increases. See Figure 2(c) for the definition of the extra pyrophyllite gasket. Curves are fitted by eye.

years, sintered diamond anvils have been tested with both the multi-anvil press and the cubic press, and much higher pressures have been obtained [22,44,45]. The sintered diamond anvils are currently very expensive though, which eventually limits their wide application.

With the large cell volume attained by the anvil-preformed gasket system, PEPs of different materials (second set of assemblies and third set of assemblies) and different sizes (fourth set of assemblies) can be employed to increase the *P*-generating capability or the *P*-generating efficiency (Figures 5–7). Recently, for example, we successfully synthesized stishovite at 800°C by using the assembly BJC5-7 (unpublished data), suggesting an experimental pressure of about 10 GPa [46]. Additionally, the large cell volume not only means large experimental samples which are crucial for the analyses of NMR, neutron diffraction, ICP-MS and so on, but also means more homogeneous temperature distribution in the sample, simply because more thermal insulating material can be employed to reduce the thermal gradient while a reasonable sample size is maintained. The early multi-anvil experiments were subjected to a temperature gradient as large as 200°C/mm along the sample length [47], and the recent ones were experienced temperature gradients in the range of 30–60°C/mm [25,48–50]. Our preliminary result suggests that the temperature gradient in our tested assemblies can be reduced down to about 15°C/mm (in preparation).

Acknowledgements

We thank Zhongjun Liu for providing some small parts and Jinguang Liu for fabricating the specially designed pyrophyllite blocks used in our experiments. We also thank Linlin Chang, Xiaomin Hu and Sicheng Wang for conducting some testing experiments with the cubic press. This investigation was financially supported by the Fundamental Research Funds for the Central Universities from the Administer of Education of P. R. China (to X. Liu) and the National Natural Science Foundation of China (Grant #41090371).

References

[1] O.F. Tuttle, *Two pressure vessels for silicate-water studies*, Geol. Soc. Am. Bull. 60 (1949), pp. 1727–1729.
[2] X. Liu and M.E. Fleet, *Phase relations of nahcolite and trona at moderate P–T conditions*, J. Mineral. Petrol. Sci. 104 (2009), pp. 25–36.
[3] H.S. Yoder Jr, *Stability relations of grossularite*, J. Geol. 58 (1950), pp. 221–253.
[4] H. Behrens and Y. Zhang, *H_2O diffusion in peralkaline to peraluminous rhyolitic melts*, Contrib. Mineral. Petrol. 157 (2009), pp. 765–780.
[5] F.R. Boyd and J.L. England, *Apparatus for phase-equilibrium measurements at pressure up to 50 kilobars and temperatures up to 1,750°C*, J. Geophys. Res. 65 (1960), pp. 741–748.
[6] X. Liu and H.St.C. O'Neill, *Partial melting of spinel lherzolite in the system CaO-MgO-Al_2O_3-$SiO_2 \pm K_2O$ at 1.1 GPa*, J. Petrol. 45 (2004), pp. 1339–1368.
[7] C. Spandler, G. Yaxley, D.H. Green, and A. Rosenthal, *Phase relations and melting of anhydrous K-bearing eclogite from 1200–1600°C and 3–5 GPa*, J. Petrol. 49 (2008), pp. 771–795.
[8] N. Kawai, and S. Endo, *The generation of ultrahigh pressures by a split sphere apparatus*, Rev. Sci. Instrum. 41 (1970), pp. 1178–1181.
[9] C.M. Bertka and Y. Fei, *Mineralogy of the Martian interior up to core-mantle boundary pressures*, J. Geophys. Res. 102 (1997), pp. 5151–5264.
[10] X. Liu, N. Nishiyama, T. Sanehira, T. Inoue, Y. Higo, and S. Sakamoto, *Decomposition of kyanite and solubility of Al_2O_3 in stishovite at high pressure and high temperature conditions*, Phys. Chem. Miner. 33 (2006), pp. 711–721.
[11] C.E. Weir, E.R. Lippincott, A. Van Valkenburg, and E.N. Bunting, *Infrared studies in the 1- to 15-micron region to 30,000 atmospheres*, J. Res. Nat. Bur. Stand. A63 (1959), pp. 55–62.
[12] H.K. Mao, P.M. Bell, J.W. Shaner, and D.J. Steinberg, *Specific volume measurements of Cu, Mo, Pd, and Ag and calibration of the ruby R1 fluorescence pressure gauge from 0.06 to 1 Mbar*, J. Appl. Phys. 49 (1978), pp. 3276–3283.
[13] X. Liu, S.R. Shieh, M.E. Fleet, and A. Akhmetov, *High-pressure study on lead fluorapatite*, Am. Mineral. 93 (2008), pp. 1581–1584.
[14] M.J. Walter and D.C. Presnall, *Melting behaviour of simplified lherzolite in the system CaO-MgO-Al_2O_3-SiO_2-Na_2O from 7 to 35 kbar*, J. Petrol. 35 (1994), pp. 329–359.
[15] J. Xu, H.K. Mao, and P.M. Bell, *High-pressure ruby and diamond fluorescence: Observations at 0.21 and 0.55 terapascal*, Science 232 (1986), pp. 1404–1406.
[16] L. Liu, *Disproportionation of kyanite to corundum plus stishovite at high pressure and high temperature*, Earth Planet. Sci. Lett. 24 (1974), pp. 224–228.

[17] C. Gao, Y. Han, Y. Ma, A. White, H. Liu, J. Luo, M. Li, C. He, A. Hao, X. Huang, Y. Pan, and G. Zou, *Accurate measurements of high pressure resistivity in a diamond anvil cell*, Rev. Sci. Instrum. 76 (2005), pp. 083912-1–5.

[18] S. Kesson, J.D. Fitz Gerald, and J.M.G. Shelley, *Mineral chemistry and density of subducted basaltic crust at lower-mantle pressures*, Nature 372 (1994), pp. 767–769.

[19] H.K. Mao, G. Shen, and R.J. Hemley, *Multivariable dependence of Fe–Mg partitioning in the lower mantle*, Science 278 (1997), pp. 2098–2100.

[20] T. Irifune, A. Yoshiharu, K. Fujino, E. Ohtani, A. Yoneda, and H. Sawamoto, *Performance test for WC anvils for multianvil apparatus and phase transformations in some aluminous minerals up to 28 GPa*, in *High-Pressure Research: Application to Earth and Planetary Sciences*, Y. Syono and M.H. Manghnani, eds., American Geophysical Union, Washington, DC, 1992, pp. 43–50.

[21] T. Katsura, K. Funakoshi, A. Kubo, N. Nishiyama, Y. Tange, Y. Sueda, T. Kubo, and W. Utsumi, *A large-volume high P–T apparatus for in situ X-ray observation, 'SPEED-MkII'*, Phys. Earth Planet. Inter. 143–144 (2004), pp. 497–506.

[22] E. Ito, D. Yamazaki, T. Yoshino, H. Fukui, S. Zhai, A. Shatzkiy, T. Katsura, Y. Tange, and K. Funakoshi, *Pressure generation and investigation of the post-perovskite transformation in $MgGeO_3$ by squeezing the Kawai-cell equipped with sintered diamond anvils*, Earth Planet. Sci. Lett. 293 (2010), pp. 84–89.

[23] D.C. Rubie, *Characterising the sample environment in multianvil high-pressure experiments*, Phase Transitions 68 (1999), pp. 431–451.

[24] F. Huang, P. Chakraborty, C.C. Lundstrom, C. Holmden, J.J.G. Glessner, S. Kieffer, and C.E. Lesher, *Isotope fractionation in silicate melts by thermal diffusion*, Nature 464 (2010), pp. 396–400.

[25] D.J. Frost, B.T. Poe, R.G. Trønnes, C. Liebske, A. Duba, and D.C. Rubie, *A new large-volume multianvil system*, Phys. Earth Planet. Inter. 143–144 (2004), pp. 507–514.

[26] K. Inoue and T. Asada, *Cubic anvil X-ray diffraction press up to 100 kbar and 1000°C*, Jpn J. Appl. Phys. 12 (1973), pp. 1786–1793.

[27] Y. Takano, N. Uchiyama, S. Ogawa, N. Môri, Y. Kimishima, S. Arisawa, A. Ishii, T. Hatano, and K. Togano, *Superconducting properties of $CuS_{2-x}Se_x$ under high pressure*, Physica C 341–348 (2000), pp. 739–740.

[28] J. Qin, D. He, J. Wang, L. Fang, L. Lei, Y. Li, J. Hu, Z. Kou, and Y. Bi, *Is rhenium diboride a superhard material?* Adv. Mater. 20 (2008), pp. 4780–4783.

[29] M. Matsui, K. Komatsu, E. Ikeda, A. Sano-Furukawa, H. Gotou, and T. Yagi, *The crystal structure of δ–Al(OH)$_3$: Neutron diffraction measurements and ab initio calculations*, Am. Mineral. 96 (2011), pp. 854–859.

[30] Q. Han, H. Ma, L. Zhou, C. Zhang, Y. Tian, X. Jia, and R. Li, *Finite element design of double bevel anvils of large volume cubic high pressure apparatus*, Rev. Sci. Instrum. 78 (2007), pp. 113906-1–3.

[31] H. Wang, D. He, N. Tan, W. Wang, J. Wang, H. Dong, H. Ma, Z. Kou, F. Peng, X. Liu, and S. Li, *Note: An anvil-preformed gasket system to extend the pressure range for large volume cubic presses*, Rev. Sci. Instrum. 81 (2010), pp. 116101-1–3.

[32] Q. Han, H. Ma, R. Li, L. Zhou, Y. Tian, Z. Liang, and X. Jia, *Finite element analysis of high-pressure anvils according to the principle of lateral support*, J. Appl. Phys. 102 (2007), pp. 084504-1–4.

[33] V.E. Bean, S. Akimoto, P.M. Bell, S. Block, W.B. Holzapfel, M.H. Manghnani, M.F. Nicol, and S.M. Stishov, *Another step toward an international practical pressure scale: 2nd AIRAPT IPPS task group report*, Physica 139 & 140B (1986), pp. 52–54.

[34] K. Kusaba, L. Galoisy, Y. Wang, M.T. Vaughan, and D.J. Weidner, *Determination of phase transition pressures of ZnTe under quasihydrostatic conditions*, Pure Appl. Geophys. 141 (1993), pp. 643–652.

[35] R. Franco, P. Mori-Sánchez, and J.M. Recio, *Theoretical compressibilities of high-pressure ZnTe polymorphs*, Phys. Rev. 68 (2003), pp. 195208-1–5.

[36] O. Degtyareva, M.I. McMahon, and R.J. Nelmes, *High-pressure structural studies of group-15 elements*, High Press. Res. 24 (2004), pp. 319–356.

[37] L. Fang, D. He, C. Chen, L. Ding, and X. Luo, *Effect of precompression on pressure-transmitting efficiency of pyrophyllite gaskets*, High Press. Res. 27 (2007), pp. 367–374.

[38] X. Liu, S. Wang, Q. He, J. Chen, H. Wang, S. Li, F. Peng, L. Zhang, and Y. Fei, *Thermal elastic behaviour of $CaSiO_3$-walstromite: A powder X-ray diffraction study up to 900°C*, Am. Mineral. 97 (2012), pp. 262–267.

[39] Q. He, X. Liu, X. Hu, S. Li, and H. Wang, *Solid solution between lead fluorapatite and lead fluorvanadate apatite: Mixing behavior, Raman feature and thermal expansivity*, Phys. Chem. Miner. 38 (2011), pp. 741–752.

[40] K. Bose and J. Ganguly, *Quartz-coesite transition revisited: Reversed experimental determination at 500–1200°C and retrieved thermochemical properties*, Am. Mineral. 80 (1995), pp. 231–238.

[41] N. Nishiyama, Y. Wang, T. Sanehira, T. Irifune, and M.L. Rivers, *Development of the multi-anvil assembly 6-6 for DIA and D-DIA type high-pressure apparatuses*, High Press. Res. 28 (2008), pp. 307–314.

[42] K. Kawazoe, N. Norimasa, Y. Nishihara, and T. Irifune, *Pressure generation to 25 GPa using a cubic anvil apparatus with a multi-anvil 6-6 assembly*, High Press. Res. 30 (2010), pp. 167–174.

[43] C.M. Sung and M. Sung, *Carbon nitrite and other speculative superhard materials*, Mater. Chem. Phys. 43 (1996), pp. 1–18.

[44] S. Endo, W. Utsumi, M. Okajima, and S. Toyoda, *High pressure and temperature experiment with sintered diamond anvil*, in *Solid State Physics under Pressure: Recent Advance with Anvil Devices*, S. Minomura, ed., KTK Scientific Publishers, Tokyo, 1985, pp. 19–24.

[45] E. Sterer and I.F. Silvera, *The c-DAD: A novel cubic diamond anvil cell with large sample volume/area and multidirectional optics*, Rev. Sci. Instrum. 77 (2006), pp. 115105-1–5.

[46] D.C. Presnall, *Phase diagrams of Earth-forming minerals*, in *Mineral Physics and Crystallography: A Handbook*

of Physical Constants, T.J. Ahrens, ed., AGU Reference Shelf 2, American Geophysical Union, Washington, D.C., 1995, pp. 248–268.

[47] E. Takahashi, H. Yamada, and E. Ito, *An ultrahigh-pressure furnace assembly to 100 kbar and 1500°C with minimum temperature uncertainty*, Geophys. Res. Lett. 9 (1982), pp. 805–807.

[48] M.J. Walter, Y. Thibault, K. Wei, and R.W. Luth, *Characterizing experimental pressure and temperature conditions in multi-anvil apparatus*, Can. J. Phys. 73 (1995), pp. 273–286.

[49] W. van Westrenen, J. Van Orman, H. Watson, Y. Fei, and E.B. Watson, *Assessment of temperature gradient in multi-anvil assemblies using spinel layer growth kinetics*, Geochem. Geophys. Geosyst. 4 (2003), pp. 1036-1–10.

[50] Y. Fei, J. Van Orman, J. Li, W. van Westrenen, C. Sanloup, W. Minarik, K. Hirose, T. Komabayashi, M. Walter, and K. Funakoshi, *Experimentally determined postspinel transformation boundary in Mg_2SiO_4 using MgO as an internal pressure standard and its geophysical implications*, J. Geophys. Res. 109 (2004), B02305-1–8.